Title	Organic-Inorganic Hybrid Nanocrystal-based Cryogels with Size- Controlled Mesopores and Macropores
Author(s)	Tarutani, Naoki; Hashimoto, Mana; Ishigaki, Takamasa
Citation	Langmuir , 37 (9) : 2884 - 2890
Issue Date	2021-02-12
DOI	10.1021/acs.langmuir.0c03112
Self DOI	
URL	https://ir.lib.hiroshima-u.ac.jp/00052860
Right	© 2021 American Chemical Society This document is the Accepted Manuscript version of a Published Work that appeared in final form in Langmuir, copyright © American Chemical Society after peer review and technical editing by the publisher. To access the final edited and published work see https://doi.org/10.1021/acs.langmuir.0c03112 This is not the published version. Please cite only the published version. この論文は出版社版ではありません。引用の際には出版社版をご確認、ご利用ください。
Relation	


Hiroshima University Institutional Repository

Organic–inorganic hybrid nanocrystal-based cryogels with size-controlled mesopores and macropores

Naoki Tarutani[†,‡,§,*], Mana Hashimoto[‡], Takamasa Ishigaki[‡,§]

[†] Applied Chemistry Program, Graduate School of Advanced Science and Engineering, Hiroshima University, 1-4-1 Kagamiyama, Higashi-Hiroshima, Hiroshima 739-8527, Japan.

[‡] Department of Chemical Science and Technology, Faculty of Bioscience and Applied Chemistry, Hosei University, 3-7-2 Kajino-cho, Koganei, Tokyo 184-8584, Japan.

[§] Research Center for Micro-Nano Technology, Hosei University, 3-11-15 Midori-cho, Koganei, Tokyo 184-8584, Japan.

KEYWORD: nanocrystals, organic-inorganic hybrid materials, radical polymerization, porous materials, cryogels

ABSTRACT: Nanocrystal-based processing has attracted significant interest for the fabrication of highly functional materials with controlled crystallinity and fine porous structures. In this study, we focused on template-free synthesis of nanocrystal-based materials with size-tailored pores using layered nickel hydroxide intercalated with acrylate anions. Polymerization of the acrylates encouraged interconnection of the nanocrystals and the formation of homogeneous gel networks. Cryogels after freeze drying had the pores with the average diameter from 4.8 nm (mesoscale) to 68.9 nm (macroscale). It was found that the surface characteristics of starting nanocrystals determined phase separation tendency of interconnected species from reaction media and resultant porous structures. We believe that the present study can enable the design of template-free nanocrystal-based porous materials.

Introduction

Over the last decades, the synthesis of nanocrystals and functional control by tuning their chemical composition, size, shape, and dispersibility have been investigated. Solution-based techniques have enabled the preparation of a variety of nanocrystals with a range of chemical compositions, such as metals, metal oxides, metal non-oxides, and metalloids.[1-6] For practical use, it is expected to assemble nanocrystals into materials with specific shapes, such as films, wires, and monolithic gels.

Bottom-up approaches using nanocrystals as nano-building blocks have attracted much attention for the design of nanocrystal-based materials.[7,8] Assembly control of nanocrystals produces unique secondary and higher-order structures, which can lead to effective use of the intrinsic nanocrystal properties and development of their extrinsic properties. For example, two different crystalline nanocubes were assembled into a bilayer structure with a large heterointerface, which displayed novel tandem catalytic properties.[9] Modification of the nanocrystal surface via functional organic molecules leads not only to the formation of assembled nanocrystal arrays but also the development of novel materials, such as thermally tunable metamaterials and acoustic metamaterials.[10,11] Assembly control of nanocrystals and the fabrication of functional materials are topics of intense interest in both the fundamental and applied sciences.[12-15]

Assembly control and interconnection of nanocrystals in three dimensions produces highly porous materials without the need for templates.[7] This strategy is based on the homogeneous destabilization of colloidal nanocrystals triggered by temperature, solvent polarity, surface ligand deprotection, and interconnection.[16] In the past, gels composed of Ti-based oxides,[17-19] metal chalcogenides,[20] metal selenides,[21] and fluoride[22] nanocrystals have been reported. Although considerable research has been carried out, the chemical compositional versatility of assembly controllable nanocrystals is still limited. In addition, structural control of the formed pores has not been achieved, which means that there remains significant scope for further progress in nanocrystal-based materials science.

In this study, we focused on layered metal hydroxide nanocrystals and controlled their assembly to form porous gels. Layered metal hydroxides are composed of electrostatically bonded metal hydroxide layers and interlayer anion layers with analogous layered structures with a wide variety of chemical compositions [23]. Owing to the chemical compositional versatility, layered metal hydroxides have been applied in many applications, such as catalysts,[24,25] adsorbents,[26,27] water oxidation,[28,29] and CO_2 capture.[30,31] Therefore, the fabrication of layered metal hydroxide nanocrystal-based porous materials is highly desired. Layered metal hydroxides grow rapidly in the lateral direction,[32] which accelerates aggregation and inhibits the formation of stable colloids. We recently developed synthesis methods to stably disperse layered metal hydroxide nanocrystals with a size

of ~2 nm.[33,34] The carboxylate anions displayed multiple functions during nucleation and crystal growth; they coordinated to the metal site, intercalated in layered structure, and adsorbed on the formed crystals, which improved the dispersibility and stability of the nanocrystal colloids. Here, layered nickel hydroxide nanocrystals with acrylate anions were employed as a model system. Nanocrystal-based porous cryogels were formed as a result of interconnection of the nanocrystals via polymerization of the acrylate anions. Systematic investigation using several types of initiator reagents and different modified nanocrystals led to the formation of nanocrystal-based cryogels with size-controlled pores ranging from the meso to macro-scale.

Experimental

Chemicals.

Nickel chloride hexahydrate ($NiCl_2 \cdot 6H_2O$, 98.0%), acrylic acid (99%), ethanol (99.5%), propylene oxide (99.0%), potassium persulfate ($K_2S_2O_8$), toluene (99.0%), 2,2'-Azobis(isobutyronitrile) (AIBN, 98.0%), 2,2'-Azobis(4-methoxy-2,4-dimethylvaleronitrile) (V-70, 95.0%), 2,2'-Azobis[2-(2-imidazolin-2-yl)propane]disulfate dihydrate (VA-046B, 97.0%), and 2-methyl-2-propanol (99.0%) were used without further purification. Acrylic acid and propylene oxide were purchased from Sigma-Aldrich Co. AIBN was purchased from Tokyo Chemical Industry Co., Ltd. All other reagents were purchased from Wako Pure Chemicals Industries, Ltd. Ultrapure water of 18.2 MΩ·cm resistivity was used in all experiments.

Preparation of nanocrystal-based porous cryogels using $K_2S_2O_8$ initiator.

$NiCl_2 \cdot 6H_2O$ (1.25 mmol) and acrylic acid were dissolved in 2.5 mL of ethanol. Propylene oxide was added to a solution and stirred for 30 s. The molar ratio of $NiCl_2 \cdot 6H_2O$, acrylic acid, and propylene oxide was 1:4:15. The resultant homogenous solutions were left at room temperature for 60 min. The obtained clear solutions were transferred to glass petri dish (φ 60 mm) and dried under vacuum conditions. As-dried powders were redispersed in water with a concentration of 200 g/L. The colloids were bubbled with N_2 at 100 mL/min for 10 min to remove dissolved oxygen. Subsequently, 0.15 mmol of $K_2S_2O_8$ was dissolved in the colloids. Wet gels were obtained after heat treated the colloids at 60 °C for 2 h. The gels were frozen at −18 °C and freeze-dried at 30 °C under vacuum conditions (~4 Pa). Freeze-dried cryogels were washed with water and dried at 40 °C.

Effect of initiator reagent on the formation of nanocrystal-based porous cryogels.

$NiCl_2 \cdot 6H_2O$ (15 mmol) and acrylic acid (30 mmol) were dissolved in 30 mL of ethanol. Propylene oxide (255 mmol) was added to a solution and stirred for 30 s. The resultant homogenous solutions were left at room temperature for 60 min. The obtained clear solutions were transferred to a glass petri dish (φ 155 mm) and dried under atmospheric pressure for 20 h. The as-dried powders were redispersed in ethanol with a concentration of 200 g/L. 0.25 mL of initiator dissolving solutions (AIBN dissolving toluene, V-70 dissolving toluene, and VA-046B dissolving methanol) (1.0 mol/L) were added to 1.0 mL of the redispersed nanocrystal colloids and left at a specific temperature for 12 h (AIBN system: 65 °C; V-70 system: 30 °C; and VA-046B system: 60 °C). The obtained gels were soaked in 2-methyl-2-propanol for washing. 2-methyl-2-propanol was exchanged with a fresh solution every hour for a total of eight times. The wet gels were frozen at 2 °C for 1 night and freeze-dried at room temperature under vacuum conditions.

Effect of nanocrystal composition on a formation of porous cryogels.

The as-dried nanocrystal powders were prepared using the same method as in section 2.2 with different nominal molar ratios of acrylic acid to $NiCl_2 \cdot 6H_2O$, $M_{AA/Ni}$ ($M_{AA/Ni}$ = 0.50–3.00). The as-dried nanocrystal powders were redispersed in ethanol with a concentration of 200 g/L. Then, 0.25 mL of V-70 dissolving toluene (1.0 mol/L) was added to 1.0 mL of the nanocrystal colloids and left at 30 °C for 12 h. The obtained gels were soaked in 2-methyl-2-propanol for washing. Then, 2-methyl-2-propanol was exchanged with a fresh solution every hour a total of eight times. The wet gels were frozen at 2 °C for one night and freeze-dried at room temperature under vacuum condition.

Characterization.

Fourier transform infrared spectroscopy (IR) spectroscopy with an attenuated total reflectance attachment (FT/IR-6600, JASCO Corp., Japan) was used to characterize the chemical bond state of the samples. Powder X-ray diffraction (XRD) measurements were used to characterize crystal phase (Cu Kα radiation, SmartLab, Rigaku, Japan). A field emission scanning electron microscope (SEM; S-8020, Hitachi, Japan) and transmission electron microscope (TEM; JEM-2010) were used to observe the nanocrystals and fine structures. The N_2 adsorption-desorption technique using a Belsorp-18 (MicrotracBEL Corp., Japan) was employed to characterize the porous structures. Samples were vacuum dried at 200 °C for 6 h prior to measurements. The specific surface area was calculated using Brunauer–Emmett–Teller theory. The pore size distribution was estimated according to the Barrett–Joyner–Halenda (BJH) method.

Results and discussion

Preparation of nanocrystal-based porous cryogels using $K_2S_2O_8$ initiator.

Preparation of the nanocrystal colloids was based on a previously reported method.[33,34] Alkalinization of the precursor metal salt solution was triggered by a ring-opening reaction of propylene oxide.[35] The incorporated acrylic acid in the precursor solution worked as a stabilizer enabling the formation of layered nickel hydroxide nanocolloids with a diameter of 3.2±0.6 nm (Fig. S1a and S1b). The as-dried powders were agglomerate of nanocrystals (Fig. S1c and 1d) and which were successfully redispersed in water (Figure S2a). The transparent green sols formed opaque wet gels after heat treatment at 60 °C for 2 h (Figure S2b), subsequently, the wet gels were freeze-dried (Figure S2c and 2d). The obtained monolithic cryogels were shaped as circular cylinders (diameter: 11.5 mm, height: 7.8 mm) with a resulting 11% shrinkage.

Figure 1a is the IR spectra of the as-dried powder (before redispersion) and the cryogel. The band at ~1560 cm^{-1} was assigned as the asymmetric bending vibration of COO,

$\nu(COO)_{as}$,[36] and they were comparable between the as-dried nanocrystals and the cryogels. The band at ~1640 cm^{-1} was assigned as the bending mode of the C=C vibration, ν(C=C), and it was not present for the cryogels. This indicates polymerization of the acrylates was initiated by $K_2S_2O_8$ during heat treatment, which led to gelation. XRD patterns of the as-dried powders and cryogels are shown in Figure 1b. The as-dried powder was assigned as acrylate intercalated layered nickel hydroxides.[34] The lattice spacing of the 00*l* plane was 1.19 nm. The cryogel showed comparable XRD patterns as the as-dried powder, which indicated that polymerization of the acrylates had little effect on the layered structure and crystallite size. The lattice spacing of 00*l* decreased to 0.93 nm. The decrease of lattice spacing consistent with reported studies,[37,38] which indicated that the configuration change of the acrylates during polymerization affected the interlayer distance.

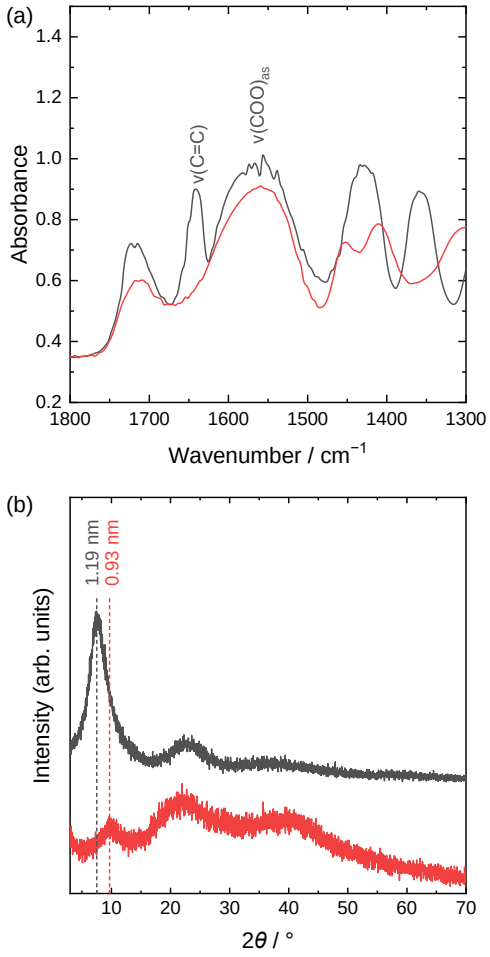

Figure 1. (a) IR spectra and (b) XRD patterns of the as-dried nanocrystal powder (black) and cryogel prepared using the $K_2S_2O_8$ initiator (red).

Figure 2 displays an SEM image of the cryogels. Pores of several micrometers in size can be observed, and the pore walls were composed of microspheres with smooth surfaces. The observed porous structure was analogous to reported porous monolithic gels with phase separated structures.[39] Based on reported layered double hydroxides-based monoliths with phase separated macropores,[40] the obtained structure was deduced as a spinodal-type phase separated structure in the later stage. To control the phase separation tendency, it is necessary to tune dispersibility of the polymeric species by changing the synthetic parameters, such as the solvent and temperature. However, the low solubility of initiator $K_2S_2O_8$ in solvents other than water limits control of phase separation tendency and the subsequent porous structures. Therefore, alternate initiators were employed to control porous structures of the nanocrystal-based gels.

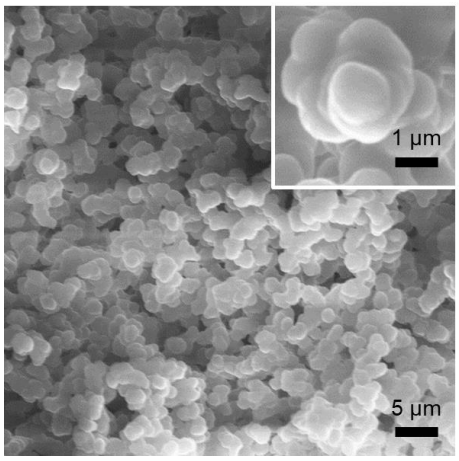

Figure 2. SEM image of cryogel prepared using the $K_2S_2O_8$ initiator. Inset is a magnified image

Effect of initiator reagent on the formation of nanocrystal-based porous cryogels.

The as-dried nanocrystals were redispersed in ethanol instead of water. Initiator dissolving toluene or methanol solutions were mixed and subsequently heat treated at a specific temperature. AIBN, V-70, and VA-046B were used to initiate polymerization of the acrylates intercalated in, coordinated to, and adsorbed on the layered nickel hydroxide nanocrystals. Figure S1 shows samples after heat treatment. There was no significant change in the case of solution heat treated at 65 °C without the initiator (Figure S3a), which indicates that the dispersibility of the individual nanocrystals was sufficiently high in ethanol during the heat treatment process. Soft opaque gels were obtained when AIBN was used as the initiator (Figure S3b), which was difficult to handle. Opaque gels were also obtained with the V-70 initiator (Figure S3c), and they were relatively rigid and maintained a monolithic shape during handling. In contrast with the former two cases, gelation did not take place when the VA-046B initiator was employed. The resultant sample was a dark brown colored solution (Figure S3d). The color change implied reaction between the nickel species and initiators.

IR spectra are shown in Figure 3. Compared with the dried powders prepared from the control solution, the absorbance of the ν(C=C) band decreased for the cryogels prepared using the AIBN and V-70 initiators. The IR spectrum of the powder prepared from the VA-046B-treated solution was comparable with the dried nanocrystal powder. To evaluate the progress of the polymerization reaction, the cumulative area ratio between the ν(C=C) and $\nu(COO)_{as}$ bands, $A_{C=C}/A_{COO}$, was calculated. The $A_{C=C}/A_{COO}$ of samples prepared using AIBN, V-70, and VA-046B were 2.0×10^{-2}, 1.7×10^{-2}, and 6.5×10^{-2}, respectively, which were smaller than or comparable to the sample prepared without

initiator (6.5×10^{-2}). The degree of the polymerization reaction determined via the $A_{C=C}/A_{COO}$ value was in good agreement with the observations (sol–gel transition) discussed above. XRD patterns of the cryogels showed layered structures with a small crystallite size (< 3 nm) (Figure S4). The interlayer distances decreased from 1.18 nm to 1.03 and 1.02 nm when using AIBN and V-70 initiators, respectively. Thus, the polymerization of the acrylates occurred when AIBN and V-70 were used as initiators. Considering the handling characteristics of the synthesized gels, V-70 was determined to be an adequate initiator for controlling the pore structure of the nanocrystal-based gels.

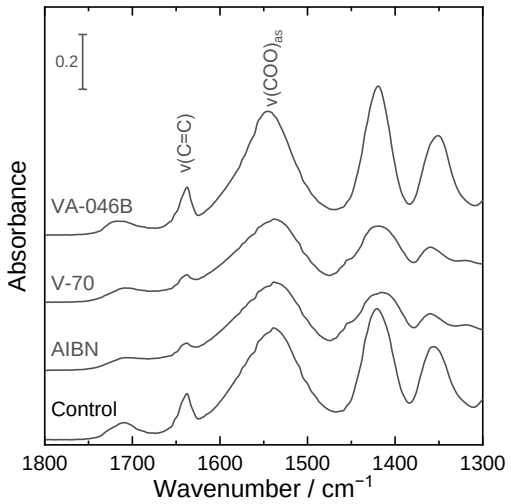

Figure 3. IR spectra of powder prepared from the control nanocrystal colloid, cryogels prepared using AIBN and V-70 initiators, and powder prepared from a solution treated with the VA-046B initiator.

Effect of nanocrystal composition on the formation of porous cryogels.

As previously reported,[34] acrylates were intercalated in, coordinated to, and adsorbed on layered hydroxides, which controlled the dispersibility of nanocrystals. In this study, the nominal molar ratios of the acrylic acid and $NiCl_2{\cdot}6H_2O$, $M_{AA/Ni}$, were changed from 0.50 to 3.00 to control the stability of the nanocrystals and the subsequent polymeric species. The synthesized nanocrystals were successfully redispersed in ethanol with a concentration of 200 g/L when $M_{AA/Ni} \geq 1.33$. Monolithic wet gels were obtained after heat treatment. The appearance of the wet gels changed from transparent to translucent to opaque depending on $M_{AA/Ni}$ (Fig. S5). The SEM images revealed that all the prepared cryogels had porous structures (Fig. S6). For the case of the transparent ($M_{AA/Ni}$ = 1.33 and 1.50) and translucent ($M_{AA/Ni}$ = 1.67) gels, numerous mesopores (diameter < 50 nm) were observed. In addition to mesopores, macropores (diameter > 50 nm) were also observed in the opaque gels ($M_{AA/Ni}$ = 2.00 and 3.00).

N_2 adsorption-desorption technique was employed to characterize porous structure. The isotherms showed type III and IV with hysteresis loops (Fig. S7a and S7b). Figure 4a and S7cshows size distribution of the pores in the cryogels. The total pore volume increased with increasing $M_{AA/Ni}$, which indicated that the nanocrystals tended to be packed more densely in the pore wall matrix, considering that the gel volumes were comparable in each system (Fig. 6a and Table S1). It is clear that the majority of the pore size distribution shifted from the macropore to mesopore scale with decreasing $M_{AA/Ni}$. The average pore diameters were 4.8 nm, 24.5 nm, and 67.6 nm for the cryogels prepared with $M_{AA/Ni}$ = 1.33, 1.67, and 3.00, respectively. The volume ratio of the mesopores and macropores is shown in Fig. 4b. The transparent and translucent gels had mesopores for over 80% of the relative pore volume, while the values in the opaque gels were ~60%. The SEM images and N_2 adsorption–desorption results indicated that the change in appearance of the wet gels from opaque to transparent derived from the decreasing pore size.

The IR band area ratio, $A_{C=C}/A_{COO}$, before and after heat treatment is plotted in Figure 5a. Before heat treatment, $A_{C=C}/A_{COO}$ had comparable values of $\sim8.0\times10^{-2}$ irrespective of $M_{AA/Ni}$. In contrast, $A_{C=C}/A_{COO}$ significantly decreased with increasing $M_{AA/Ni}$ after heat treatment. This indicated that the polymerization degree of the acrylate species was high at large $M_{AA/Ni}$. Densification of the nanocrystals was assumed to accelerate the polymerization reaction. The XRD patterns of the cryogels are shown in Fig. S8. All the XRD patterns were assigned as acrylate/polyacrylate intercalated layered nickel hydroxides. The 00*l* lattice spacing is shown in Fig. 5b. While the lattice spacings were comparable before and after heat treatment for the case of $M_{AA/Ni} \leq$ 1.67, gels with $M_{AA/Ni} \geq 2.00$ showed a significant decrease in the lattice spacing. This trend was consistent with that of the polymerization degree deduced from the IR spectra.

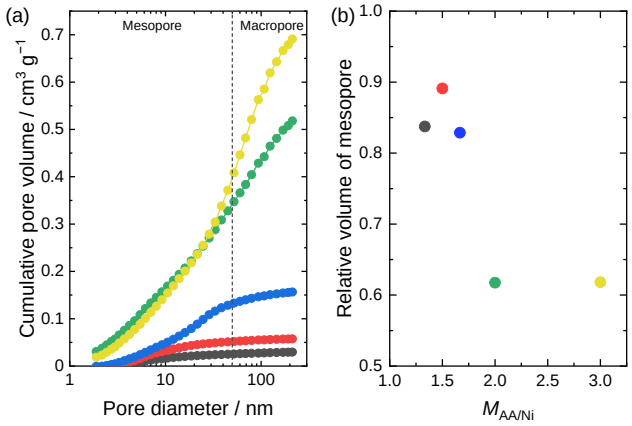

Figure 4. (a) Pore size distribution and (b) volume ratio of the mesopores and macropores of the cryogels prepared using the V-70 initiator with $M_{AA/Ni}$ = 1.33 (black), 1.50 (red), 1.67 (blue), 2.00 (green), and 3.00 (yellow).

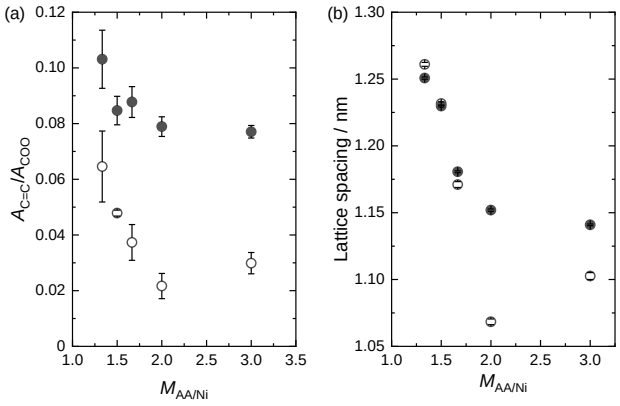

Figure 5. (a) Band area ratio of ν(C=C) and ν(COO) calculated from the IR spectra and (b) lattice spacing of the 00*l* plane calculated from XRD patterns of the as-dried powders (close) and cryogels (open) prepared using V-70 initiator with $M_{AA/Ni}$ = 1.33–3.00.

A hypothetical mechanism for pore size change with $M_{AA/Ni}$ is shown in Figure 6. For the case of $M_{AA/Ni} \leq 1.50$, the OH ligands were assumed as the majority on the surface of nanocrystals. Interconnection of the nanocrystals proceeded via polymerization of the acrylates, and the formed interconnected species may be stably dispersed in ethanol because of its high hydrophilicity. As a result, transparent gels composed of a thin interconnected network of nanocrystals with mesopores were obtained. In contrast, acrylate ligands significantly increased when $M_{AA/Ni} \geq 2.00$. Here, polymerization of the acrylates and interconnection of the nanocrystals might proceed rapidly. The formed interconnected species will be relatively hydrophobic compared with $M_{AA/Ni} \leq 1.50$, which would trigger and accelerate phase separation. Networks of densely packed nanocrystals leave macropores, and the resultant gels were opaque. The gels were rigid because of the thick highly polymerized skeletons. Translucent gels were obtained for the case of $1.50 < M_{AA/Ni} < 2.00$ based on an intermediate polymerization and phase separation tendency.

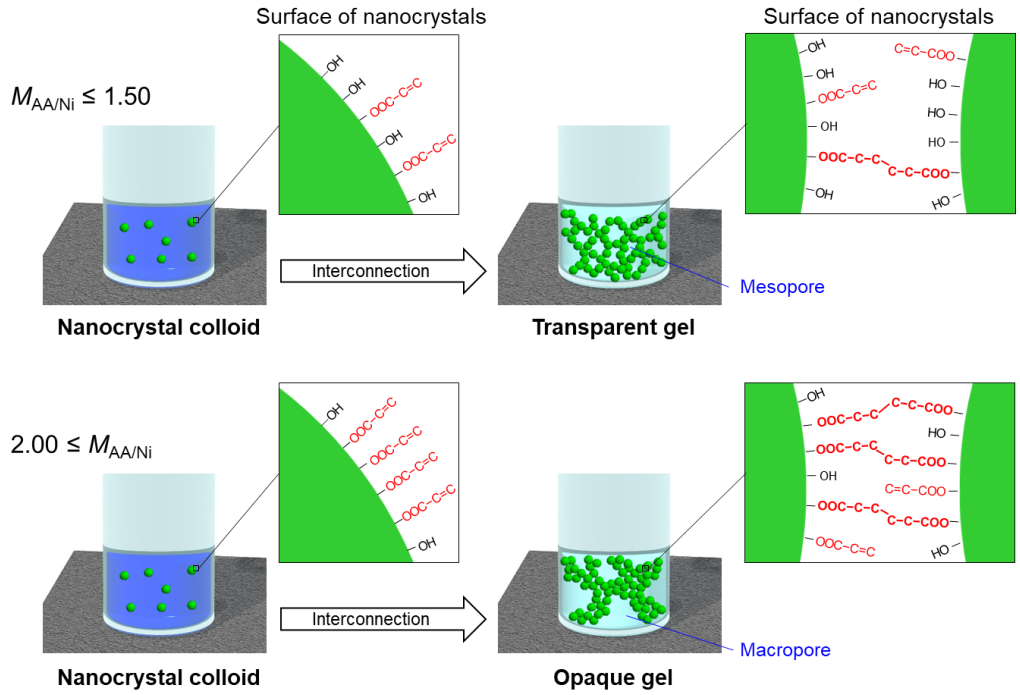

Figure 6. Schematic illustration of a formation mechanism for the mesoporous and macroporous cryogels through interconnection of nanocrystals by polymerization of acrylate.

Conclusion

In this study, nanocrystal-based porous cryogels were prepared via polymerization of coordinated/intercalated/adsorbed acrylate anions. Layered nickel hydroxide nanocrystals with acrylates were prepared by an epoxide-mediated alkalinization process. The polymerization of the acrylates was triggered by radical initiators resulting in interconnected nanocrystals. The nanocrystal networks were homogeneously distributed, which hindered precipitation and led to the formation of monolithic gels. Porous cryogels were obtained after freeze-drying. It was found that the type of radical initiator affected the robustness of the wet gels. Systematic change of the surface characteristics of the nanocrystals enabled tuning of the assembly tendency and resulting pore size. Depending on the solution philicity of the nanocrystals, the pore size distribution in the cryogels gradually shifted from a majority being in the mesoscale to the macroscale. The pore size control of nanocrystal-based gels in this study will enable to design the functions of the materials, such as adsorption, catalytic, electrochemical properties because macropores will control diffusion of

liquid/ions and mesopores will control number of accessible active sites.

ASSOCIATED CONTENT

Supporting Information. Photo images, XRD patterns, and SEM images.

AUTHOR INFORMATION

Corresponding Author

* E-mail: n-tarutani@hiroshima-u.ac.jp

ACKNOWLEDGMENT

The present work was partially supported by JSPS KAKENHI Grant Number JP20K15368, MEXT Leading Initiative for Excellent Young Researchers, the Foundation for the Promotion of Ion Engineering, and the Izumi Science and Technology Foundation (2019-J-112). We thank Arun Paraecattil, PhD, from Edanz Group (https://en-author-services.edanzgroup.com/ac) for editing a draft of this manuscript.

REFERENCES

(1) Jana, N. R.; Chen, Y.; Peng, X. Size- and Shape-Controlled Magnetic (Cr, Mn, Fe, Co, Ni) Oxide Nanocrystals via a Simple and General Approach. *Chem. Mater.* **2004**, *16* (20), 3931–3935. https://doi.org/10.1021/cm049221k.

(2) Pang, X.; He, Y.; Jung, J.; Lin, Z. 1D Nanocrystals with Precisely Controlled Dimensions, Compositions, and Architectures. *Science (80-.).* **2016**, *353* (6305), 1268–1272. https://doi.org/10.1126/science.aad8279.

(3) Murray, C. B.; Norris, D. J.; Bawendi, M. G. Synthesis and Characterization of Nearly Monodisperse CdE (E = S, Se, Te) Semiconductor Nanocrystallites. *J. Am. Chem. Soc.* **1993**, *115* (19), 8706–8715. https://doi.org/10.1021/ja00072a025.

(4) Talapin, D. V.; Lee, J.-S.; Kovalenko, M. V.; Shevchenko, E. V. Prospects of Colloidal Nanocrystals for Electronic and Optoelectronic Applications. *Chem. Rev.* **2010**, *110* (1), 389–458. https://doi.org/10.1021/cr900137k.

(5) Malgras, V.; Henzie, J.; Takei, T.; Yamauchi, Y. Stable Blue Luminescent CsPbBr3 Perovskite Nanocrystals Confined in Mesoporous Thin Films. *Angew. Chemie - Int. Ed.* **2018**, *57* (29), 8881–8885. https://doi.org/10.1002/anie.201802335.

(6) Wu, C. W.; Yamauchi, Y.; Ohsuna, T.; Kuroda, K. Structural Study of Highly Ordered Mesoporous Silica Thin Films and Replicated Pt Nanowires by High-Resolution Scanning Electron Microscopy (HRSEM). *J. Mater. Chem.* **2006**, *16* (30), 3091–3098. https://doi.org/10.1039/b604062d.

(7) Niederberger, M. Multiscale Nanoparticle Assembly: From Particulate Precise Manufacturing to Colloidal Processing. *Adv. Funct. Mater.* **2017**, *27* (47), 1–18. https://doi.org/10.1002/adfm.201703647.

(8) Xue, Z.; Yan, C.; Wang, T. From Atoms to Lives: The Evolution of Nanoparticle Assemblies. *Adv. Funct. Mater.* **2019**, *29* (12), 1–33. https://doi.org/10.1002/adfm.201807658.

(9) Yamada, Y.; Tsung, C. K.; Huang, W.; Huo, Z.; Habas, S. E.; Soejima, T.; Aliaga, C. E.; Somorjai, G. A.; Yang, P. Nanocrystal Bilayer for Tandem Catalysis. *Nat. Chem.* **2011**, *3* (5), 372–376. https://doi.org/10.1038/nchem.1018.

(10) Lewandowski, W.; Fruhnert, M.; Mieczkowski, J.; Rockstuhl, C.; Górecka, E. Dynamically Self-Assembled Silver Nanoparticles as a Thermally Tunable Metamaterial. *Nat. Commun.* **2015**, *6*. https://doi.org/10.1038/ncomms7590.

(11) Yazdani, N.; Jansen, M.; Bozyigit, D.; Lin, W. M. M.; Volk, S.; Yarema, O.; Yarema, M.; Juranyi, F.; Huber, S. D.; Wood, V. Nanocrystal Superlattices as Phonon-Engineered Solids and Acoustic Metamaterials. *Nat. Commun.* **2019**, *10* (1), 1–6. https://doi.org/10.1038/s41467-019-12305-3.

(12) Ducrot, É.; He, M.; Yi, G. R.; Pine, D. J. Colloidal Alloys with Preassembled Clusters and Spheres. *Nat. Mater.* **2017**, *16* (6), 652–657. https://doi.org/10.1038/nmat4869.

(13) McMillan, J. R.; Brodin, J. D.; Millan, J. A.; Lee, B.; Olvera de la Cruz, M.; Mirkin, C. A. Modulating Nanoparticle Superlattice Structure Using Proteins with Tunable Bond Distributions. *J. Am. Chem. Soc.* **2017**, *139* (5), 1754–1757. https://doi.org/10.1021/jacs.6b11893.

(14) Cui, J.; Panfil, Y. E.; Koley, S.; Shamalia, D.; Waiskopf, N.; Remennik, S.; Popov, I.; Oded, M.; Banin, U. Colloidal Quantum Dot Molecules Manifesting Quantum Coupling at Room Temperature. *Nat. Commun.* **2019**, *10* (1), 5401. https://doi.org/10.1038/s41467-019-13349-1.

(15) Geuchies, J. J.; Van Overbeek, C.; Evers, W. H.; Goris, B.; De Backer, A.; Gantapara, A. P.; Rabouw, F. T.; Hilhorst, J.; Peters, J. L.; Konovalov, O.; Petukhov, A. V.; Dijkstra, M.; Siebbeles, L. D. A.; Van Aert, S.; Bals, S.; Vanmaekelbergh, D. In Situ Study of the Formation Mechanism of Two-Dimensional Superlattices from PbSe Nanocrystals. *Nat. Mater.* **2016**, *15* (12), 1248–1254. https://doi.org/10.1038/nmat4746.

(16) Ziegler, C.; Wolf, A.; Liu, W.; Herrmann, A. K.; Gaponik, N.; Eychmüller, A. Modern Inorganic Aerogels. *Angew. Chemie - Int. Ed.* **2017**, *56* (43), 13200–13221. https://doi.org/10.1002/anie.201611552.

(17) Heiligtag, F. J.; Rossell, M. D.; Süess, M. J.; Niederberger, M. Template-Free Co-Assembly of Preformed Au and TiO2 Nanoparticles into Multicomponent 3D Aerogels. *J. Mater. Chem.* **2011**, *21* (42), 16893–16899. https://doi.org/10.1039/c1jm11740h.

(18) Rechberger, F.; Ilari, G.; Niederberger, M. Assembly of Antimony Doped Tin Oxide Nanocrystals into Conducting Macroscopic Aerogel Monoliths. *Chem. Commun.* **2014**, *50* (86), 13138–13141. https://doi.org/10.1039/c4cc05648e.

(19) Rechberger, F.; Heiligtag, F. J.; Süess, M. J.; Niederberger, M. Assembly of BaTiO 3 Nanocrystals into Macroscopic Aerogel Monoliths with High Surface Area. *Angew. Chemie Int. Ed.* **2014**, *53* (26), 6823–6826. https://doi.org/10.1002/anie.201402164.

(20) Arachchige, I. U.; Brock, S. L. Sol–Gel Methods for the Assembly of Metal Chalcogenide Quantum Dots. *Acc. Chem. Res.* **2007**, *40* (9), 801–809. https://doi.org/10.1021/ar600028s.

(21) Sayevich, V.; Cai, B.; Benad, A.; Haubold, D.; Sonntag, L.; Gaponik, N.; Lesnyak, V.; Eychmüller, A. 3D Assembly of All-Inorganic Colloidal Nanocrystals into Gels and Aerogels. *Angew. Chemie Int. Ed.* **2016**, *55* (21), 6334–6338. https://doi.org/10.1002/anie.201600094.

(22) Odziomek, M.; Chaput, F.; Lerouge, F.; Dujardin, C.; Sitarz, M.; Karpati, S.; Parola, S. From Nanoparticle Assembly to Monolithic Aerogels of YAG, Rare Earth Fluorides, and Composites. *Chem. Mater.* **2018**, *30* (15), 5460–5467. https://doi.org/10.1021/acs.chemmater.8b02443.

(23) Miyata, S.; Kumura, T. Synthesis of New Hydrotalcite-Like Compounds and Their Physico-Chemical Properties. *Chem. Lett.* **1973**, *2* (8), 843–848. https://doi.org/10.1246/cl.1973.843.

(24) Yan, K.; Liu, Y.; Lu, Y.; Chai, J.; Sun, L. Catalytic Application of Layered Double Hydroxide-Derived Catalysts for the Conversion of Biomass-Derived Molecules. *Catal. Sci. Technol.* **2017**, *7* (8), 1622–1645. https://doi.org/10.1039/C7CY00274B.

(25) Bing, W.; Zheng, L.; He, S.; Rao, D.; Xu, M.; Zheng, L.; Wang, B.; Wang, Y.; Wei, M. Insights on Active Sites of CaAl-Hydrotalcite as a High-Performance Solid Base Catalyst toward Aldol Condensation. *ACS Catal.* **2018**, *8* (1), 656–664. https://doi.org/10.1021/acscatal.7b03022.

(26) Kuroda, Y.; Yamaguchi, K.; Kuroda, K.; Mizuno, N. Relationship between Aggregated Structures and Dispersibility of Layered Double Hydroxide Nanoparticles ca. 10nm in Size and Their Application to Ultrafast Removal of Aqueous Anionic Dye. *Bull. Chem. Soc. Jpn.* **2015**, *88* (12), 1765–1772. https://doi.org/10.1246/bcsj.20150271.

(27) Jia, Y. H.; Liu, Z. H. Preparation of Borate Anions Intercalated MgAl-LDHs Microsphere and Its Calcinated Product with

Superior Adsorption Performance for Congo Red. *Colloids Surfaces A Physicochem. Eng. Asp.* **2019**, *575* (March), 373–381. https://doi.org/10.1016/j.colsurfa.2019.05.032.

(28) Wang, Z.; Long, X.; Yang, S. Effects of Metal Combinations on the Electrocatalytic Properties of Transition-Metal-Based Layered Double Hydroxides for Water Oxidation: A Perspective with Insights. *ACS Omega* **2018**, *3* (12), 16529–16541. https://doi.org/10.1021/acsomega.8b02565.

(29) Huang, L.; Chen, R.; Xie, C.; Chen, C.; Wang, Y.; Zeng, Y.; Chen, D.; Wang, S. Rapid Cationic Defect and Anion Dual-Regulated Layered Double Hydroxides for Efficient Water Oxidation. *Nanoscale* **2018**, *10* (28), 13638–13644. https://doi.org/10.1039/c8nr04402c.

(30) Ram Reddy, M. K.; Xu, Z. P.; Lu, G. Q.; Da Costa, J. C. D. Layered Double Hydroxides for CO2 Capture: Structure Evolution and Regeneration. *Ind. Eng. Chem. Res.* **2006**, *45* (22), 7504–7509. https://doi.org/10.1021/ie060757k.

(31) Yang, Z. zhu; Wei, J. jing; Zeng, G. ming; Zhang, H. qing; Tan, X. fei; Ma, C.; Li, X. cheng; Li, Z. hao; Zhang, C. A Review on Strategies to LDH-Based Materials to Improve Adsorption Capacity and Photoreduction Efficiency for CO 2. *Coord. Chem. Rev.* **2019**, *386*, 154–182. https://doi.org/10.1016/j.ccr.2019.01.018.

(32) Soler-Illia, G. J. de A. A.; Jobbágy, M.; Regazzoni, A. E.; Blesa, M. A. Synthesis of Nickel Hydroxide by Homogeneous Alkalinization. Precipitation Mechanism. *Chem. Mater.* **1999**, *11* (11), 3140–3146. https://doi.org/10.1021/cm9902220.

(33) Tarutani, N.; Tokudome, Y.; Jobbágy, M.; Viva, F. A.; Soler-Illia, G. J. A. A.; Takahashi, M. Single-Nanometer-Sized Low-Valence Metal Hydroxide Crystals: Synthesis via Epoxide-Mediated Alkalinization and Assembly toward Functional Mesoporous Materials. *Chem. Mater.* **2016**, *28* (16), 5606–5610. https://doi.org/10.1021/acs.chemmater.6b02510.

(34) Tarutani, N.; Tokudome, Y.; Jobbágy, M.; Soler-Illia, G. J. A. A.; Tang, Q.; Müller, M.; Takahashi, M. Highly Ordered Mesoporous Hydroxide Thin Films through Self-Assembly of Size-Tailored Nanobuilding Blocks: A Theoretical-Experimental Approach. *Chem. Mater.* **2019**, *31* (2), 322–330. https://doi.org/10.1021/acs.chemmater.8b03082.

(35) Gash, A. E.; Tillotson, T. M.; Satcher, J. H.; Poco, J. F.; Hrubesh, L. W.; Simpson, R. L. Use of Epoxides in the Sol - Gel Synthesis of Porous Iron (III) Oxide Monoliths from Fe (III) Salts. *Chem. Mater.* **2001**, *13* (Iii), 999–1007. https://doi.org/10.1021/cm0007611.

(36) Feairheller, W. R.; Katon, J. E. The Vibrational Spectra of Acrylic Acid and Sodium Acrylate. *Spectrochim. Acta Part A Mol. Spectrosc.* **1967**, *23* (8), 2225–2232. https://doi.org/10.1016/0584-8539(67)80114-4.

(37) Poul, L.; Jouini, N.; Fievet, F. Layered Hydroxide Metal Acetates (Metal = Zinc, Cobalt, and Nickel): Elaboration via Hydrolysis in Polyol Medium and Comparative Study. *Chem. Mater.* **2000**, *12* (10), 3123–3132. https://doi.org/10.1021/cm991179j.

(38) Vaysse, C.; Guerlou-Demourgues, L.; Duguet, E.; Delmas, C. Acrylate Intercalation and in Situ Polymerization in Iron-, Cobalt-, or Manganese-Substituted Nickel Hydroxides. *Inorg. Chem.* **2003**, *42* (15), 4559–4567. https://doi.org/10.1021/ic026229s.

(39) Nakanishi, K. Pore Structure Control of Silica Gels Based on Phase Separation. *J. Porous Mat.* **1997**, *4* (2), 67–112. https://doi.org/10.1023/A:1009627216939.

(40) Tokudome, Y.; Tarutani, N.; Nakanishi, K.; Takahashi, M. Layered Double Hydroxide (LDH)-Based Monolith with Interconnected Hierarchical Channels: Enhanced Sorption Affinity for Anionic Species. *J. Mater. Chem. A* **2013**, *1* (26), 7702–7708. https://doi.org/10.1039/c3ta11110e.

TOC

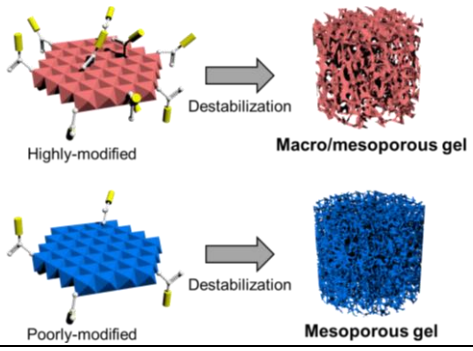
Destabilization
Highly-modified
Macro/mesoporous gel
Destabilization
Poorly-modified
Mesoporous gel